3-1-1997

Far-Ultraviolet Absorption Lines in the Remnant of SN 1006

Chi-Chao Wu
Space Telescope Science Institute

D. Michael Crenshaw
NASA/Goddard Space Flight Center

Andrew J. S. Hamilton
University of Colorado Boulder

Robert A. Fesen
Dartmouth College

THE ASTROPHYSICAL JOURNAL, 477:L53–L56, 1997 March 1

FAR-ULTRAVIOLET ABSORPTION LINES IN THE REMNANT OF SN 1006[1]

CHI-CHAO WU,[2] D. MICHAEL CRENSHAW,[3] ANDREW J. S. HAMILTON,[4]
ROBERT A. FESEN,[5] MARVIN LEVENTHAL,[6] AND CRAIG L. SARAZIN[7]
Received 1996 June 28; accepted 1996 December 17

ABSTRACT

We have obtained a far-ultraviolet spectrum (1150–1600 Å) of a hot subdwarf star behind the remnant of supernova 1006 with the Faint Object Spectrograph (FOS) on the *Hubble Space Telescope*. The high-quality spectrum is used to test previous identifications of the strong absorption features discovered with the *International Ultraviolet Explorer*. These features have FWHM = 4000 (±300) km s^{-1} and are not at the rest wavelengths of known interstellar lines, as opposed to the broader (∼8000 km s^{-1} FWHM) Fe II lines from the remnant centered at 0 km s^{-1} in near-UV FOS spectra. We confirm that the broad absorption features are principally due to redshifted Si II, Si III, and Si IV lines, which are centered at a radial velocity of 5100 (±200) km s^{-1}.

The Si II λ1260.4 profile is asymmetric, with a nearly flat core and sharp red wing, unlike the Si II λ1526.7 and Si IV λλ1393.8, 1402.8 profiles. One possible explanation is additional absorption from another species. Previous work has suggested that S II λλ1250.6, 1253.8, 1259.5 at a radial velocity of ∼6000 km s^{-1} is responsible, but this would require a sulfur-to-silicon abundance ratio that is at least a factor of 10 higher than expected. Another possible explanation is that the Si II and Si IV profiles are intrinsically different, but this does not explain the symmetric (albeit weaker) Si II λ1526.7 profile.

Subject headings: ISM: abundances — ISM: individual (SN 1006) — supernova remnants

1. INTRODUCTION

A hot subdwarf star (the "SM star") discovered by Schweizer & Middleditch (1980) lies on the far side of the remnant of supernova (SN) 1006 and provides an unusual opportunity to study its ejecta in absorption. *IUE* observations (Wu et al. 1983; Fesen et al. 1988) revealed the presence of strong, broad Fe II absorption lines centered at zero velocity. Subsequent Faint Object Spectrograph (FOS) spectra (Wu et al. 1993) were obtained at a sufficient signal-to-noise ratio and resolution to remove the narrow interstellar and stellar lines, deblend the broad Fe II lines, and determine an intrinsic Fe II profile that is suitable for comparison with model predictions for Type Ia supernovae. The Fe II velocity profile is roughly symmetric around 0 km s^{-1} and extends up to about ±8000 km s^{-1} at the continuum. The absorption-line width and angular size of the remnant yield a lower limit to the distance of 1.9 kpc (more recent estimates based on the NW optical filament's proper motion and shock velocity yield 1.8 ± 0.3 kpc; see Laming et al. 1996). Whereas the remnant contains approximately 0.014 $M_\odot$ of Fe^+, the predicted mass of Fe from Type Ia supernova models (Nomoto, Thielemann, & Yokoi 1984; Höflich & Khokhlov 1996) is about 25 times this value. However, most of the Fe in supernova remnant (SNR) 1006 could be in higher ionization states than Fe II (Hamilton & Fesen 1988; Blair, Long, & Raymond 1996).

The *IUE* observations also showed strong, broad absorption lines in the far-UV, but these features were not at the rest wavelengths of known interstellar lines. Wu et al. (1983) proposed that the outer portions of the ejecta are less chemically processed. They identified the features as Si II, Si III, and Si IV lines originating from a clump in the far side of the ejecta, which is moving at a radial velocity of ∼5000 km s^{-1}. Based on a spectrum of SN 1006 with the *Hopkins Ultraviolet Telescope* (*HUT*), Blair et al. (1996) attribute these lines entirely to Si. However, Fesen et al. (1988) showed that the wavelength correspondences are not exact, the line strengths are not quite in the expected ratios, and some of the lines are asymmetric, and they suggested that S II at ∼6000 km s^{-1} and O I at ∼6500 km s^{-1} may also contribute to these features. Fesen et al. (1988) suggested that these features may arise from clumps of shocked material composed of intermediate mass elements in the far side of the ejecta. We have obtained high signal-to-noise spectra of the far-UV lines to test these identifications, and we present the most likely interpretations of these features. A companion paper (Hamilton et al. 1996) presents a detailed physical picture of the ejecta based on one of these interpretations.

2. OBSERVATIONS AND MEASUREMENTS

FOS observations of the SM star behind SNR 1006 were obtained on 1993 September 17–20, prior to the installation of COSTAR on *HST*, through a circular aperture with a projected diameter of 1″ (which gives instrumental profiles that are nearly Gaussian; see Kinney 1992). The FOS/BLUE detector and G130H grating were used to obtain a total integration time of 468 min over the range 1150–1600 Å at a resolution of $\lambda/\Delta\lambda \approx 1000$. The positions of the strong interstellar lines indicate that no correction to the wavelength scale

[1] Based on observations with the NASA/ESA *Hubble Space Telescope*, obtained at the Space Telescope Science Institute, which is operated by the Association of Universities for Research in Astronomy, Inc., under NASA contract NAS5-26555.

[2] Computer Sciences Corporation, Space Telescope Science Institute, 3700 San Martin Drive, Baltimore, MD 21218; wu@stsci.edu.

[3] Computer Sciences Corporation, Laboratory for Astronomy and Solar Physics, Code 681, NASA/Goddard Space Flight Center, Greenbelt, MD 20771.

[4] University of Colorado, JILA, Box 440, Boulder, CO 80309.

[5] Dartmouth College, Department of Physics and Astronomy, 6127 Wilder Hall, Hanover, NH 03755.

[6] University of Maryland, Department of Astronomy, College Park, MD 20742-2421.

[7] University of Virginia, Department of Astronomy, P.O. Box 3818, Charlottesville, VA 22903.

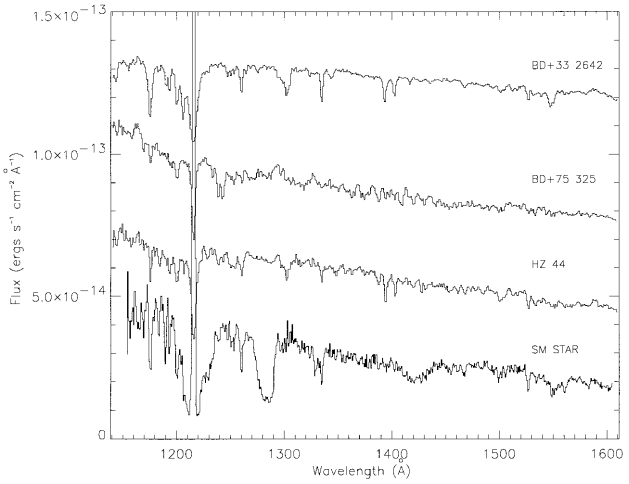

FIG. 1.—Observed FOS G130H spectra of the SM star behind SNR 1006 and standard stars HZ 44 (sdO), BD +75°325 (sdO), and BD +33°2642 (B2 IV). Each standard star spectrum has been scaled to the same average flux as the dereddened $S-M$ spectrum and subsequently offset by adding a constant positive flux.

was needed. The absolute flux scale of the G130H spectrum was adjusted by multiplying the fluxes by a constant factor of 1.08, in order to match the FOS G190H fluxes in the 30 Å region of overlap. The spectrum of the SM star was binned to an interval of one-half resolution element (∼0.7 Å), for comparison with standard star spectra (generously provided by Ralph Bohlin). Based on photon counting statistics, the signal-to-noise ratios per half-resolution element in the continuum of the SM star spectrum are ∼30 at $\lambda > 1250$ Å and drop steadily below 1250 Å to ∼10 at 1150 Å.

Figure 1 shows the observed spectrum of the SM star behind SNR 1006 and scaled spectra of hot standard stars. The spectra of HZ 44 (sdO) and BD +75°325 (sdO) are useful for identifying stellar features, and the spectrum of BD +33°2642 (B2 IV) is helpful for identifying interstellar features. Comparison of our FOS spectrum with the *HUT* spectrum of the SM star (Blair et al. 1996), obtained over the range 912–1840 Å, shows good agreement at $\lambda > 1300$ Å. At $\lambda < 1300$ Å the spectra begin to diverge, with the FOS continuum showing an excess of ∼20% over the *HUT* continuum at ∼1200 Å. This may indicate a problem with the FOS calibration at the shortest wavelengths; further comparison of standard stars observed with *HUT* and FOS is needed to investigate this problem.

The observed FOS spectrum was dereddened using a value of $E_{B-V} = 0.1$, which was determined from the 2200 Å depression in the continuum (Wu et al. 1993) and the interstellar extinction curve of Savage & Mathis (1979). The narrow interstellar and stellar absorption lines were measured and removed as described in Wu et al. (1993). All narrow lines were measured directly using a local continuum; each line with an equivalent width greater than 3 times the expected error was retained for further analysis. The narrow lines were remeasured with a Gaussian fitting routine to determine better positions (accurate to about ±0.5 Å), equivalent widths, and errors in the equivalent widths, and they were then removed from the FOS spectrum by subtracting the appropriate Gaussian fits. Table 1 lists the narrow lines that were measured. All of the strong interstellar lines that are expected (Morton 1991) are seen; most of the remaining narrow absorption features are difficult to identify unambiguously at this resolution but are very likely blends of lines that are common in hot subdwarf stars, such as C III, C IV, N III, Fe IV, and Fe V (Bruhweiler, Kondo, & McCluskey 1981; Dean & Bruhweiler 1985). Each feature that has been measured is also seen in at least one of the hot subdwarf spectra.

Figure 1 shows that in addition to the narrow stellar and interstellar lines in the spectrum of the SM star, the broad absorption features from the SNR seen by Wu et al. (1983) and Fesen et al. (1988) are present at the following approximate positions: 1217, 1282, 1331, 1421, and 1553 Å. The position (i.e., centroid), equivalent width, and velocity width (FWHM) of each of these features were determined using a linear fit to local continuum points. One σ errors in the measurements were determined from the photon noise and different reasonable placements of the continuum and the flux and wavelength extremes. Table 2 gives these measurements and errors.

The positions and equivalent widths of the broad lines in Table 2 are essentially the same as those in Wu et al. (1983) and Fesen et al. (1988), who identify these features as principally redshifted Si lines. The central radial velocities in Table 2 are calculated from these identifications and the measured positions. The absorption feature at 1217 Å (see Fig. 1) has contributions from geocoronal Lyα emission, stellar and interstellar Lyα absorption, redshifted Si II λλ1190.4, 1193.3 ab-

TABLE 1

NARROW ABSORPTION-LINE MEASUREMENTS

λ (Å)	Equivalent Widths (Å)	σ_{EW} (Å)	Identification	λ (Å)	Equivalent Widths (Å)	σ_{EW} (Å)	Identification
1175.7	1.14	0.19	C III λ1175.7 (stellar)	1328.4	0.23	0.09	C I λ1328.8
1183.8	0.44	0.12		1334.6	0.53	0.13	C II λ1334.5
1189.8	0.78	0.12	Si II λ1190.4	1454.9	0.21	0.05	
1193.5	0.66	0.08	Si II λ1193.3	1460.5	0.16	0.06	
1200.2	1.22	0.10	N I λ1200	1466.7	0.49	0.13	
1206.7	0.55	0.11	Si III λ1206.5	1499.1	0.41	0.10	
1229.5	0.27	0.11		1505.3	0.22	0.06	
1239.4	0.23	0.07		1526.6	0.61	0.08	Si II λ1526.7
1247.4	0.18	0.05		1534.1	0.31	0.07	
1250.6	0.30	0.10	S II λ1250.6	1538.5	0.16	0.07	
1253.4	0.52	0.11	S II λ1253.8	1548.4	0.34	0.07	C IV λ1548.2
1260.0	1.06	0.12	Si II λ1260.4	1550.8	0.29	0.06	C IV λ1550.8
1296.4	0.18	0.06	S I λ1295.8	1560.5	0.25	0.06	C I λ1560.3
1301.8	0.13	0.05	O I λ1302.2	1582.7	0.31	0.08	
1304.2	0.13	0.08	Si II λ1304.4				

TABLE 2

BROAD FAR-UV ABSORPTION LINES IN SNR 1006

λ (Å)	Equivalent Width (Å)	FWHM (km s^{-1})	Identification	v_r (km s^{-1})
1217.0 ± 1.0	20.9 ± 1.7	...	Si II λλ1190.4, 1193.3; Si III λ1206.5; stellar Lyα	...
1282.3 ± 0.4	10.5 ± 0.6	3900 ± 200	Si II λ1260.4; residual absorption?	5200 ± 100
1330.6 ± 3.0	1.7 ± 0.4	3400 ± 900	Si II λ1304.4; residual absorption?	6000 ± 700
1421.2 ± 0.4	4.9 ± 0.7	4000 ± 300	Si IV λλ1393.8, 1402.8	4900 ± 100
1552.9 ± 0.5	3.2 ± 0.3	4200 ± 200	Si II λ1526.7	5100 ± 100

sorption, and redshifted Si III λ1206.5 absorption. Because of the blending of these lines, no values are given for their widths and radial velocities in Table 2. The 1331 Å feature is weak and contaminated by strong narrow interstellar lines, so the corresponding errors are large. The width and radial velocity of each component of the Si IV λλ1393.8, 1402.8 doublet were derived using the template profile fit described below.

3. INTERPRETATION OF THE BROAD LINES

The broad absorption features in Table 2 are at the same radial velocity (5100 ± 200 km s^{-1}) and have the same width (4000 ± 300 km s^{-1} FWHM, errors determined from the dispersion in values and the individual measurement errors). Thus we confirm that these features are primarily due to broad redshifted Si II, Si III, and Si IV lines. Further evidence based on the strengths and profiles of the lines is presented below, along with possible evidence of additional absorption from other species.

Figure 2 shows expanded plots of the broad absorption features from the dereddened spectrum, including the profiles prior to and after removal of the narrow lines. The basic purpose of this plot is to compare the strengths and profiles of the absorption features, to determine if they can be interpreted in a consistent manner. The 1282 Å feature represents the strongest Si II line according to Table 2, so its profile is adopted for comparison with the other lines. This feature was normalized to the local continuum to create a template profile, assuming that it is entirely due to redshifted Si II λ1260.4. The template was then reproduced at the expected positions of the Si II λ1304.4 and λ1526.7 lines (at a radial velocity of $v_r = 5100$ km s^{-1}) using the oscillator strengths for these lines (Morton 1991). The template was also reproduced at the expected positions of the Si IV λλ1393.8, 1402.8 and Si III λ1206.5 lines, but the scale factors were varied to provide the best fit to the observed profiles. The scaled templates at the local continuum levels are shown in Figure 2 for comparison with the actual absorption features.

First we consider the Si II absorption lines, which should have the same profiles. The close correspondence between the 1282 Å template and the 1553 Å feature, without the need for further scaling, indicates that these features are indeed primarily due to Si II λ1260.4 and Si II λ1526.7. There is some evidence for additional broad absorption in the 1282 Å feature, in the core and just redward of the core. Comparison of the SM star spectrum with the hot subdwarf spectra in Figure 1 indicates that there are no strong stellar or interstellar lines that could be responsible for the excess broad absorption in the 1282 Å feature. The 1553 Å feature has substantial contamination by narrow lines, but tests using different scaling factors for their removal do not result in a better agreement of the profiles. A straightforward interpretation is that the difference in profiles is due to additional absorption in the 1282 Å feature.

For the 1331 Å feature, the scaled template is at least consistent with the presence of Si II λ1304.4 absorption, given the noisiness of this feature. There may be additional absorption from another species as well, even in excess of that present in the 1282 Å template. However, the presence of strong narrow interstellar lines in this region complicate the interpretation of this feature, and it is possible that a larger contribution from the C I and C II lines could explain more of the excess absorption.

For the 1421 Å feature, the template was reproduced at the positions of the individual Si IV components and scaled to the blue wing. There is also evidence for additional absorption in the 1282 Å feature, in the same location as noted before. However, another possibility is that the Si II and Si IV profiles are intrinsically different (Hamilton et al. 1996).

The complicated nature of the 1217 Å feature makes it

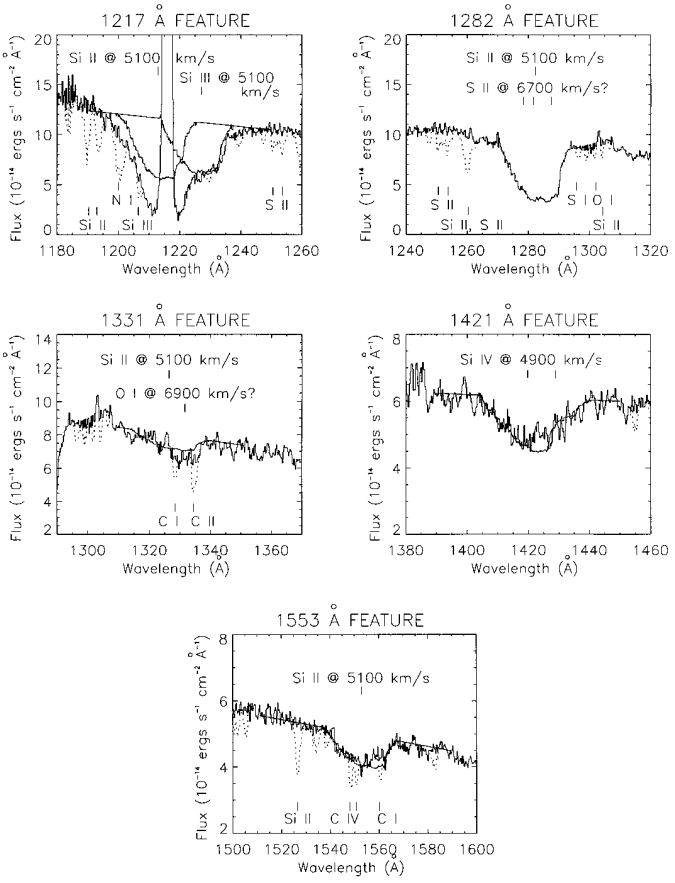

FIG. 2.—Expanded plots of the dereddened FOS spectrum of the SM star. The dotted and solid lines give the spectra prior to and after the removal of the narrow absorption lines, respectively. The smooth solid lines are the scaled 1282 Å template at the expected positions of the redshifted Si II, Si III, and Si IV lines. Narrow interstellar lines and broad SNR lines are labeled below and above the spectra, respectively (question marks indicate uncertain identifications).

difficult to obtain an accurate deconvolution. However, the Si III line is sufficiently distinct to provide an estimate of its strength by fitting the red wing of the feature. The poor match of the template to the blue wing of this feature is a concern; it may be due to an error in the flux calibration in this region, as discussed earlier.

We conclude that previous work is correct in the identification of Si II, Si III, and Si IV as the main contributors to the broad absorption lines in the far-UV. In addition, these lines have the same approximate radial velocities and widths, despite the range in ionization level. However, the profiles of the features attributed to Si II are dissimilar.

As noted by Fesen et al. (1988), a possible explanation for the different Si II profiles is the presence of additional absorption in the 1282 Å and 1331 Å features, and they suggest that S II λλ1250.6, 1253.8, 1259.5 and O I λ1303.2 lines may be responsible. The positions and widths needed for these lines to reproduce the observed features were determined from an estimate of the excess absorption. The corresponding radial velocities are noted in Figure 2. If the residual absorptions are interpreted as S II and O I lines, they are at the same approximate radial velocity (∼6800 km s^{-1}), which is substantially higher than that of the Si lines. Although the residuals are noisy, they are clearly narrower than the Si lines (∼1800 km s^{-1}). The next section points out the difficulties in this interpretation.

4. DISCUSSION

An interesting result from the FOS observations is the large intrinsic width of the far-UV absorption lines from SNR 1006, which might be expected to resolve into individual components if the absorption arises from small knots of gas. In fact, the profiles of the deblended Si lines start at v_r = 1500 (±500) km s^{-1} and extend out to v_r = 8500 (±500) km s^{-1}, which is close to the extent of the red wing of the Fe II lines (at ∼8000 km s^{-1}). This suggests that the Si lines arise not from a small clump or a few clumps of material but rather in a layer of gas in bulk motion in the far side of the ejecta and that Si and Fe may be intermixed on the far side. We note that there is substantial observational and theoretical evidence for mixing of the interior and exterior layers in a Type II supernova (SN 1987A; see Bussard, Burrows, & The 1989; Yamada & Sato 1991).

The equivalent widths of the broad absorption lines have not varied at the ≥20% level over ∼12 years of UV observation, since the first *IUE* observations by Wu et al. (1983). This lack of variability is also difficult to reconcile with small clumps, which have significant transverse velocities because the hot subdwarf is ∼2.′5 from the center of the SNR. From the 12 year time interval, projected offset of the subdwarf, and observed velocities, a lower limit of 0.02 pc is obtained for the size of the absorbing region perpendicular to the line of sight.

Another interesting result from the FOS spectra is that there is no evidence for strong blueshifted counterparts to the redshifted Si lines (although there appears to be a weak depression in the ∼1375 Å region, just blueward of the Si IV λλ1393.8 line). The lack of blueshifted Si lines can be explained by asymmetry in the original supernova explosion and/or asymmetry in the distribution of the interstellar medium surrounding the supernova (along with a significant interaction of the ejecta with the interstellar medium). Hamilton et al. (1996) discuss these possibilities in detail and argue for a much lower density of the interstellar medium on the far side of the remnant compared with the rest of the remnant.

The apparent excess absorptions in the 1282 Å and 1331 Å features are difficult to understand. They may be interpreted as S II and O I lines with centroids at higher redshifted radial velocities, but then the relative abundance of sulfur would have to be much higher than predicted from models of Type Ia supernovae. The column densities of the Si ions, determined from direct integration of the optical depths across the profiles, are N(Si II) = 6.7 (±0.6) × 10^{14} cm^{-2}, N(Si III) = 3.1 (±0.6) × 10^{14} cm^{-2}, and N(Si IV) = 3.6 (±0.5) × 10^{14} cm^{-2}. (The Si II value comes from Si II λ1526.7 at 1553 Å, whereas Hamilton et al. [1996] obtain a higher value by assuming the entire 1282 Å feature is due to Si II λ1260.4.) The column densities of the S II and O I lines, estimated from the excess absorption, can be used to determine a lower limit to their abundance relative to the total Si abundance (assuming no other ionization states for Si). The ratio of oxygen to silicon abundance is ≥1, which is close to the expected ratio of 1–2 (Nomoto et al. 1984). The ratio of sulfur to silicon abundance is ≥5.5, which is a factor of 10 higher than the expected ratio of ∼0.5 (Nomoto et al. 1984). Thus, although the identification of the silicon lines is secure, the interpretation of excess absorption due to redshifted sulfur and oxygen lines is in doubt.

Hamilton et al. (1996) discuss an alternate interpretation of the 1282 Å feature, in which the asymmetric profile is due to shocked and unshocked components of Si II λ1260.4 absorption. However, this does not explain the difference between the observed Si II λ1260.4 and Si II λ1526.7 line profiles. Since the present FOS data are insufficient to resolve this apparent discrepancy, observations at higher resolution (to fit and remove the narrow lines more accurately) and higher signal-to-noise ratio (to get better profiles of the weak broad lines) are desirable. Improved data will also set stricter limits on blueshifted absorption features from the remnant's approaching hemisphere. Similar observations of a hot subdwarf star that is chosen to match the effective temperature and surface gravity of the SM star would also be helpful in determining an accurate continuum and removing stellar absorption features.

This work was supported by STScI grant GO-3621.01-91A to the Computer Sciences Corporation. We thank the referee for helpful comments.

REFERENCES

Blair, W. P., Long, K. S., & Raymond, J. C. 1996, ApJ, 468, 871
Bruhweiler, F. C., Kondo, Y., & McCluskey, G. E. 1981, ApJS, 46, 255
Bussard, R. W., Burrows, A., & The, L. S. 1989, ApJ, 341, 401
Dean, C. A., & Bruhweiler, F. C. 1985, ApJS, 57, 133
Fesen, R. A., Wu, C.-C., Leventhal, M., & Hamilton, A. J. S. 1988, ApJ, 327, 164
Hamilton, A. J. S., & Fesen, R. A. 1988, ApJ, 327, 178
Hamilton, A. J. S., Fesen, R. A., Wu, C.-C., Crenshaw, D. M., & Sarazin, C. L. 1996, ApJ, in press
Höflich, P., & Khokhlov, A. 1996, ApJ, 457, 500
Kinney, A. L. 1992, *Hubble Space Telescope* Faint Object Spectrograph Instrument Handbook, Version 2.0
Laming, J. M., Raymond, J. C., McLaughlin, B. M., & Blair, W. P. 1996, ApJ, 472, 267
Morton, D. C. 1991, ApJS, 77, 119
Nomoto, K., Thielemann, F.-K., & Yokoi, K. 1984, ApJ, 286, 644
Savage, B. D., & Mathis, J. S. 1979, ARA&A, 17, 73
Schweizer, F., & Middleditch, J. 1980, ApJ, 241, 1039
Wu, C.-C., Crenshaw, D. M., Fesen, R. A., Hamilton, A. J. S., & Sarazin, C. L. 1993, ApJ, 416, 247
Wu, C.-C., Leventhal, M., Sarazin, C. L., & Gull, T. R. 1983, ApJ, 269, L5
Yamada, S., & Sato, K. 1991, ApJ, 382, 594